

EFFECT OF HVOF PARAMETER ON TITANIUM OXIDE (TiO₂) COATING CHARACTERISTICS ON AZ81 MAGNESIUM ALLOY

Muthuraj Marimuthu^{1*}, Rama Thirumurugan², Ashokkumar Mohankumar³ and Mathanbabu Mariappan⁴

¹Department of Mechanical Engineering, Akshaya College of Engineering and Technology, Coimbatore, Tamil Nadu 642109, India

²Department of Mechanical Engineering, Dr. Mahalingam College of Engineering and Technology, Pollachi, Tamil Nadu-642003, India

³Centre for sustainable materials and surface metamorphosis, Chennai Institute of Technology, Chennai-600069, Tamil Nadu, India

⁴Department of Mechanical Engineering, Government College of Engineering, Bargur, Tamil Nadu-635104, India

(Received May 8, 2024; Revised July 27, 2024; Accepted July 30, 2024)

ABSTRACT. High-velocity oxy-fuel (HVOF) coating to enhance the erosion, wear, and corrosion-resistant properties crucial for orthopedic applications. HVOF is distinguished for its capability to provide surfaces with a dense and superior finish. Porosity and hardness serve as vital process variables in assessing performance. This current study aims to optimize HVOF process parameters to minimize porosity values in titanium oxide (TiO₂) coatings applied on AZ81 magnesium substrate. Oxygen flow, liquefied petroleum gas (LPG) flow, coating material feed rate, and spray distance were selected due to their significant impact on the coating quality. Statistical techniques such as response surface methodology (RSM), analysis of variations, and design of experiments (DoE) were employed to obtain the necessary results. The findings indicate that LPG flow has the most significant influence on coating quality, followed by standoff distance, oxygen flow rate, and feed rate. The coating obtained using optimal spray parameters exhibits a lower surface porosity of 0.86 vol.% and achieves a greater hardness of 922 HV. This has been confirmed through validation via the response graph. Consequently, the optimized parameters for TiO₂ deposit entail an oxygen flow rate of 266 lpm, an LPG flow rate of 68 lpm, a powder feed rate of 35 g/min, and a spray distance of 236 mm.

KEY WORDS: High-velocity oxy-fuel, Response surface methodology, Porosity, Hardness, AZ81 Magnesium alloy, Titanium oxide

INTRODUCTION

Titanium oxide (TiO₂) is among the most analyzed minerals, owing to its exceptional qualities in several uses, including photocatalytic activity, photoelectronic devices, hydrogen generation, conventional medicine, and corrosive resistance [1]. It acts as a coating to improve the adhesion of the succeeding layers. Sol-gel, electrophoretic deposition, immerse-and-revolve coating, plasma spraying techniques, and electrophoretic deposition are some of the documented methods to produce these forms of coating. [2-4]. Thermal spray-deposited TiO₂ coatings have been investigated as a unique layer as well as a BC that optimizes the surface adhesion of upper coats to metal surfaces [5–11]. The HVOF treatment proved to optimize overall adhesion and the fracture dispersion, tension, and wear resistance of the coatings, one of the various thermal spray methods. [12-14]. In the high-velocity oxygen fuel procedure, the in-flight particulates that hit the base are flattened and hardened in an array of dimensions and shapes to create disc-like forms, or splats, which are the required fundamental building blocks for the coating development technique.

The collision of in-flight particulates also causes additional effects, including the development of groups of semi- and non-fused particles, splashes, rebounds, and imprinting caused by the

*Corresponding authors. E-mail: muthurajphd24@gmail.com, irrttmuthu89@gmail.com
This work is licensed under the Creative Commons Attribution 4.0 International License

prediction of non-fused particles [15]. The stand-off distance (SOD), powder feed rate, fuel proportion, number of passes, distribution of particle sizes, and overall gas flow are some of the thermal spray diffusion variables that impact the properties of the spatter and surface coating, like adhesion, elemental composition, microstructure, etc.

Titanium (Ti) is presently the most extensively utilized substance in the field of orthopedics [16, 17]. The potential uses of these materials encompass micro-plates, micro-bone-screws, prosthetic bone joints, and delicate surgical equipment. Titanium-based ceramics provide numerous exceptional characteristics, such as reduced density, enhanced strength, corrosion resistance, favourable biological compatibility, compatibility with magnetic fields, and absence of allergic responses following implants [18]. TiO₂ represents the inherent oxide layer of titanium (Ti). While TiO₂ does not possess inherent antibacterial capabilities, it presents numerous prospects for enhancing the efficacy of titanium as a biomedical implant. Furthermore, the fabrication of TiO₂ nanostructures with enhanced osteogenic characteristics compared to Ti is considered advantageous. In addition, the utilization of TiO₂ has the potential to enhance the level of bone-implant interaction through the stimulation of cellular activity.

The use of TiO₂ deposition on surgical magnesium substrates offers numerous benefits in biomedical engineering. TiO₂ enhances biocompatibility, reducing adverse reactions upon implantation. It acts as a protective barrier against corrosion, extending the implant lifespan. Moreover, TiO₂ coatings improve surface properties, promoting cell adhesion and tissue integration, thus facilitating accelerated healing. Additionally, they can be engineered for controlled drug release, aiding in tissue regeneration and infection prevention. Overall, TiO₂-coated magnesium implants mitigate inflammation and immune responses, leading to better patient outcomes. This versatile approach enhances implant performance, biocompatibility, and longevity, making them suitable for diverse surgical applications [19].

The primary aim of this research study is to examine and enhance the HVOF spraying variables employed during the deposition of TiO₂ onto surgery Mg substrate. The powder feed rate and fuel proportion are known to affect flow rate, temperature, or coating grade for all these parameters [20–23]. Important information about the separation process and its relationship to the characteristics of the last covering is provided by the connection between the temperature and speed of in-flight particulates and the coating variables, which combine process mapping and experimental design (DoE), which incorporates the analysis of variance (ANOVA) [24–31].

From the previously published papers [2-21], a lot of studies on optimizing the HVOF process parameter on Mg alloys, and the data was scattered. As of now, there is no model available to predict the coatings characteristics of HVOF sprayed TiO₂ on AZ81D Mg Alloy. An effort was made to carry out on optimizing the high-velocity oxy-fuel (HVOF) spray parameters of TiO₂ coatings on AZ81D Mg alloy. The leading issue in the production of coatings using the HVOF is finding the optimum input parameters to attain the desired coating properties on AZ81D Mg alloy for biomedical implants.

EXPERIMENTAL

This study utilized 2.5 mm thickness of wide sheets of magnesium as the base material. The chemical components of the AZ81 magnesium substrate 8.071Al; 1Zn; 0.209Mn; 0.012 Cu; 0.010 Fe; 0.002 Ni; 0.042 Si. The current investigation uses crushed TiO₂ as a coating materials. The crushed titanium oxide (TiO₂) was acquired from Spray Met Surface Technologies Pvt. Ltd., Bangalore. Ball milling was done for one hour at 150 rpm, with 25% of the container volume occupied and a ball-to-weight ratio of 1:1. The powder was then simply used for spraying after being sieved using a vibratory screening machine to acquire feedstock particle sizes of ~ 17µm. XRD analysis using CuKα radiation was used to examine the coating phase composition. A comprehensive scan was carried out using a step size of 0.002 mm and a step period of 0.3 seconds, with 2θ values spanning from 200 to 1000.

Fabrication of TiO₂ coating

Equipment from Spraymet Surface Technologies Pvt. Ltd., Bangalore, was used to perform the HVOF coating, in which a high-velocity jet was utilized by the ignition of an LPG and oxygen blend. For the TiO₂ coating, the spraying conditions used throughout the HVOF coating were optimized. The AZ81 magnesium specimens were separated from their as-received state, grit bombarded with corundum grits measuring 530 μm, cleaned with acetone in an ultrasound bath, and then cured. The average surface roughness following sandblasting was determined to be 5 to 10 μm by a surface roughness tester (Make: Mitutoyo, Japan; model Surf Test 301). The HVOF spraying system and uncoated and coated specimens are illustrated in Figure 1, respectively. During the coatings, Coating thickness was measured using an Elcometer (Model: Elcometer 456) for each pass of the HVOF gun during the coatings. Additionally, the average thickness of the cross-sections was measured from different 10 places of the cross-section using an optical microscope equipped with image analyzing software.

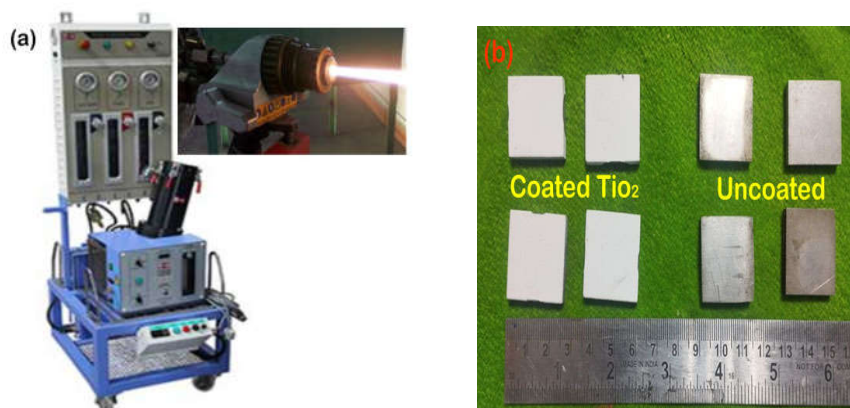


Figure 1. Experimental setup.

Porosity analysis

The permeability and fracture toughness of the coatings were measured using metallographic cross-sections. The coated specimens had first been meticulously sliced to the necessary proportions using a sluggish crystallographic sample saw (Make: Ducom, India; Model: MSS-10) equipped with an epoxy-sharp cutting disc (10x10 mm). Particles were then attached using the lowest-viscosity epoxy adhesive in a vacuum atmosphere. The attached samples were then progressively crushed with SiC papers of 600, 800, 1000, and 1500 grit before being polished throughout 5, 5, 10, and 10 minutes, respectively, with diamond slurries of 10-8, 9-5, 5-2, 2-0.5, and 0.5-0 micron. It's challenging to quantify and evaluate true permeability in metallographically created spray coverings due to pullouts in brittle materials. If the microstructural grinding and polishing aren't done properly, something that isn't part of the coating structure may be introduced. Because ceramic coatings are fragile, during grinding, particles might come loose from the surface. These breakouts provide the erroneous impression of significant porosity if they are not adequately polished. Using an optical microscope, the coatings' microstructures were examined on their surface and in their cross-section (OM). On the polished cross-section of the covering, the permeability of the coatings was evaluated by ASTM E2109-11 standards with the help of an

optical microscope (Make: Meiji; Japan, Model: MIL-7100) fitted with a photographic-analysis system (Meta vision version 6). The right magnification must be used during image analysis to catch aspects of photographs, including large pores, voids, and connectivity breaks. In this study, a 200 m² area of that smoothed and polished cross-sectional area on the coverings was selected for porosity study at 400x intensity of optical morphology with a resolution of 1024 x 768 picture elements, and the picture was examined. To estimate the mean proportional area of permeability, the very same process was carried out ten times at random sites.

Microhardness testing

A Vickers microhardness tester (make: Shimadzu; Japan) Model HMV-2T) was used to assess the coatings' microhardness. To determine the hardness, a 300 g load and a dwell period of 15 s were used. On the polished cross-section of the coating, at ten random locations, the hardness values were measured.

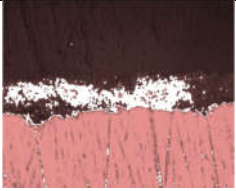
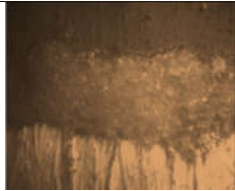
Selection of the key process parameters

Picking variables that indicate process conditions is the first step in the design of operations. The thermal spray business is aware that a huge number of variables could have an impact on the characteristics of the coating. The main factors influencing the effects of the deposition process were discovered from the publications and tests done in our lab. The following are the standard HVOF process variables: Spraying range, rate of powder feed, oxygen, and LPG flow rate.

Recognizing the process parameters' practical limits

AZ81 substrate pieces that had been grit blasted, various spraying experiments were performed to establish the acceptable operating range of the HVOF processing parameters by adjusting one parameter while maintaining the others fixed. Trial tests are properly carried out, and Table 1 shows the outcomes. The procedure factor's maximum and minimum limits, which are illustrated in Table 2, were determined based on the findings.

Table 1. Microstructural observations during HVOF sprayed TiO₂ coating trials.

Parameter	Level	Micrograph	Observation
Oxygen flow rate	< 254 lpm 50 μm		Poor adhesion of the coating Coating delamination
	>270 lpm 50 μm		Fragmentation and small solidified splats


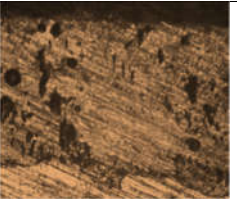
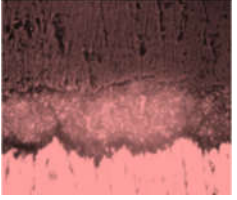
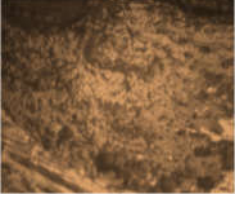
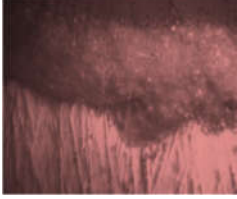

LPG Flow rate	<64 lpm 50 μm		More unmelted particles along with melted region
	>80 lpm 50 μm		Pores, voids, and splashing of particles observed
Powder feed rate	<30 gpm 50 μm		Poor deposition of particles
	>50 gpm 50 μm		More unmelted particles
Spray distance	<218 mm 50 μm		Dense and thick unmelted particles
	>242 mm 50 μm		Poor deposition due to loss of sprayed particles

Table 2. Important HVOF spray parameters.

No	Factor	Units	Levels				
			-2	-1	0	1	2
1	Oxygen flow rate (T)	lpm	254	258	262	266	270
2	LPG flow rate (Q)	lpm	64	68	72	76	80
3	Powder feed rate (R)	g/min	30	35	40	45	50
4	Spray distance (S)	mm	218	224	230	236	242

Developing the experimental design matrix

By keeping in mind the given factors, it was possible to pick characteristic boundaries that resulted in a remarkably adhesive HVOF spray coating. The main composite rotatable, four-component, five-level model structure was selected due to the wide variety of different factors. A much-improved technique in Response Surface Methodology (RSM) for defining the important correlation that the scholars have emphasized with the fewest tests permitted without compromising quality has been discovered to be a centralized composite rotatable layout of the secondary order. Table 3 lists the 30 groups of coded parameters that were utilized to create the design matrix. From the layout pattern, the main 16 test circumstances are calculated. The combos of every process parameter at the least (-2) or most (+2) value with the remaining four factors at varying levels create the star, whereas all the elements at their moderate level (0) from the center points. The evaluation of the linear, quadratic, and two-way interaction impacts of such factors upon the permeability and micro-hardness within the HVOF sprayed covering was therefore achieved by the 30 test conditions. The greater and lesser levels of the determinants were conveniently recorded as (-2) and (+2) for recording and processing the experimental results.

The continuity equation can be used to determine the data for a number of transitory variables:

$$H_i = 2 \left[2H - (H_{max} + H_{min}) \right] / [H_{max} - H_{min}] \quad (1)$$

where, H_i is the needed coded value of a factor H , H is any value of the factor from H_{min} to H_{max} , H_{min} is the lowest level of the factor; and H_{max} is the highest level of the factor.

Table 3. Design matrix experimental results.

Run	Coded value				Original value				Responses	
	T	Q	R	S	T	Q	R	S	Porosity	Hardness
1	-1	-1	-1	-1	258	68	35	224	3	755
2	1	-1	-1	-1	266	68	35	224	1.65	850
3	-1	1	-1	-1	258	76	35	224	1.69	830
4	1	1	-1	-1	266	76	35	224	1.32	913
5	-1	-1	1	-1	258	68	45	224	3.72	744
6	1	-1	1	-1	266	68	45	224	1.62	834
7	-1	1	1	-1	258	76	45	224	1.37	885
8	1	1	1	-1	266	76	45	224	1.6	872
9	-1	-1	-1	1	258	68	35	236	3.37	784
10	1	-1	-1	1	266	68	35	236	0.86	922
11	-1	1	-1	1	258	76	35	236	3	781
12	1	1	-1	1	266	76	35	236	2	845

13	-1	-1	1	1	258	68	45	236	4	663
14	1	-1	1	1	266	68	45	236	3.5	745
15	-1	1	1	1	258	76	45	236	3.6	735
16	1	1	1	1	266	76	45	236	2.87	783
17	-2	0	0	0	254	72	40	230	3.56	726
18	2	0	0	0	270	72	40	230	1.8	864
19	0	-2	0	0	262	64	40	230	3.57	717
20	0	2	0	0	262	80	40	230	1.94	829
21	0	0	-2	0	262	72	30	230	1.53	876
22	0	0	2	0	262	72	50	230	3.59	797
23	0	0	0	-2	262	72	40	218	1.94	879
24	0	0	0	2	262	72	40	242	3.54	751
25	0	0	0	0	262	72	40	230	1.17	896
26	0	0	0	0	262	72	40	230	1.24	901
27	0	0	0	0	262	72	40	230	1.17	892
28	0	0	0	0	262	72	40	230	1.8	898
29	0	0	0	0	262	72	40	230	1.06	891
30	0	0	0	0	262	72	40	230	1.14	903

Development of a predictive model for tio2 coating

A response surface approach was employed in the current project to estimate the response porosity as well as the micro-toughness of HVOF-applied coatings. Response surface methodology, a mathematical and data analysis technique combo based on a limited number of experiments, is good for developing, enhancing, and refining the HVOF process. A second-degree polynomial equation was created to forecast the outcomes of tests using various combinations.

The outcomes are a function of spraying range, rate of powder feed, oxygen, and LPG flow, and they can be shown as:

$$\text{Outcomes} = f(T, Q, R, S) \quad (2)$$

A quadratic model with multiple factors seems to have the following general form:

$$M = c_0 + \sum c_{ii}x_i + \sum c_{ii}x_i^2 + \sum c_{uv}x_u x_v \quad (3)$$

The selected polynomial equation for the four factors can be derived as below:

$$M = c_0 + c_{01}(T) + c_{02}(Q) + c_{03}(R) + c_{04}(S) + c_{11}(T^2) + c_{22}(Q^2) + c_{33}(R^2) + c_{44}(S^2) + c_{12}(TQ) + c_{13}(TR) + c_{14}(TS) + c_{23}(QR) + c_{24}(QS) + c_{34}(RS)$$

where c_0 is the average of responses and $c_{01}, c_{02}, c_{03}, \dots, c_{44}$ are predictor variables that relate to the corresponding linear, interaction, and square terms of variables. Software called Design Experiment was used to estimate the coefficient's value. The overall empirical relationship was created by employing the coefficients (at a 95% confidence level) that had been determined. Below is the complete statistical model used to estimate the answers in following equations.

$$\begin{aligned} \text{Porosity of the deposit} = & 2.1 - 0.3T - 0.30Q + 0.38R + 0.42TS + 0.27TQ + 0.12TR - 0.06QS - 0.13QR \\ & + 0.21RS + 0.23S + 0.29T^2 + 0.31Q^2 + 0.26R^2 + 0.31S^2 \quad (\text{vol}\%) \end{aligned} \quad (4)$$

$$\begin{aligned} \text{Hardness of the deposit} = & 890.4 + 34.5T + 26.5Q - 18.4R - 31.1S - 7.3TQ - 2.9TR - 0.61TS \\ & + 13QR - 15.3QS - 23.2RS - 23.9T^2 - 29.4Q^2 + 13.5R^2 - 18.9S^2 \quad (HV) \end{aligned} \quad (5)$$

Checking the adequacy of the developed model

The analysis of variance (ANOVA) approach has been utilized to figure out whether the generated empirical relationship was sufficient. In this analysis, 95% confidence was deemed to be the optimum level of assurance. If (a) the value obtained from the developed model's "Q" percentage does not outpace the basic calculated value of that fraction "Q" and (b) the output obtained from the developed relationship's "R" fraction exceeds the basic calculated value of that ratio at the preferred suitable level, the relationship may be deemed sufficient. The model is determined to be suitable. The probability > F value in Table 4 indicates that the model is strong.

Table 4. ANOVA test results for hardness and porosity.

ANOVA test results for hardness						
Source	Sum of squares	df	Mean square	F-value	p-value	
Model	1.580E+05	14	11286.03	17.39	< 0.0001	Significant
A-T	37052.04	1	37052.04	57.11	< 0.0001	
B-Q	17658.37	1	17658.37	27.22	0.0001	
C-R	17985.38	1	17985.38	27.72	< 0.0001	
D-S	24130.04	1	24130.04	37.19	< 0.0001	
AB	1278.06	1	1278.06	1.97	0.1808	
AC	4000.56	1	4000.56	6.17	0.0253	
AD	0.5625	1	0.5625	0.0009	0.9769	
BC	1425.06	1	1425.06	2.20	0.1590	
BD	8418.06	1	8418.06	12.97	0.0026	
CD	6123.06	1	6123.06	9.44	0.0077	
A ²	15757.74	1	15757.74	24.29	0.0002	
B ²	23819.17	1	23819.17	36.71	< 0.0001	
C ²	5068.53	1	5068.53	7.81	0.0136	
D ²	9869.17	1	9869.17	15.21	0.0014	
Residual	9732.58	15	648.84			
Lack of Fit	9617.75	10	961.78	41.88	0.0003	Not significant
Pure Error	114.83	5	22.97			
Cor Total	1.677E+05	29				
ANOVA test results for porosity						
Source	Sum of squares	df	Mean square	F-value	p-value	
Model	28.23	14	2.02	13.23	< 0.0001	Significant
A-T	5.85	1	5.85	38.38	< 0.0001	
B-Q	2.36	1	2.36	15.50	0.0013	
C-R	3.77	1	3.77	24.72	0.0002	
D-S	4.53	1	4.53	29.73	< 0.0001	
AB	1.32	1	1.32	8.64	0.0102	
AC	0.2836	1	0.2836	1.86	0.1927	
AD	0.0827	1	0.0827	0.5422	0.4729	
BC	0.4001	1	0.4001	2.62	0.1261	
BD	0.8789	1	0.8789	5.77	0.0298	
CD	1.05	1	1.05	6.86	0.0194	
A ²	2.72	1	2.72	17.84	0.0007	
B ²	3.05	1	3.05	20.03	0.0004	
C ²	2.23	1	2.23	14.60	0.0017	
D ²	2.99	1	2.99	19.58	0.0005	
Residual	2.29	15	0.1525			
Lack of Fit	1.92	10	0.1924	2.65	0.1465	Not significant
Pure Error	0.3625	5	0.0725			
Cor Total	30.52	29				

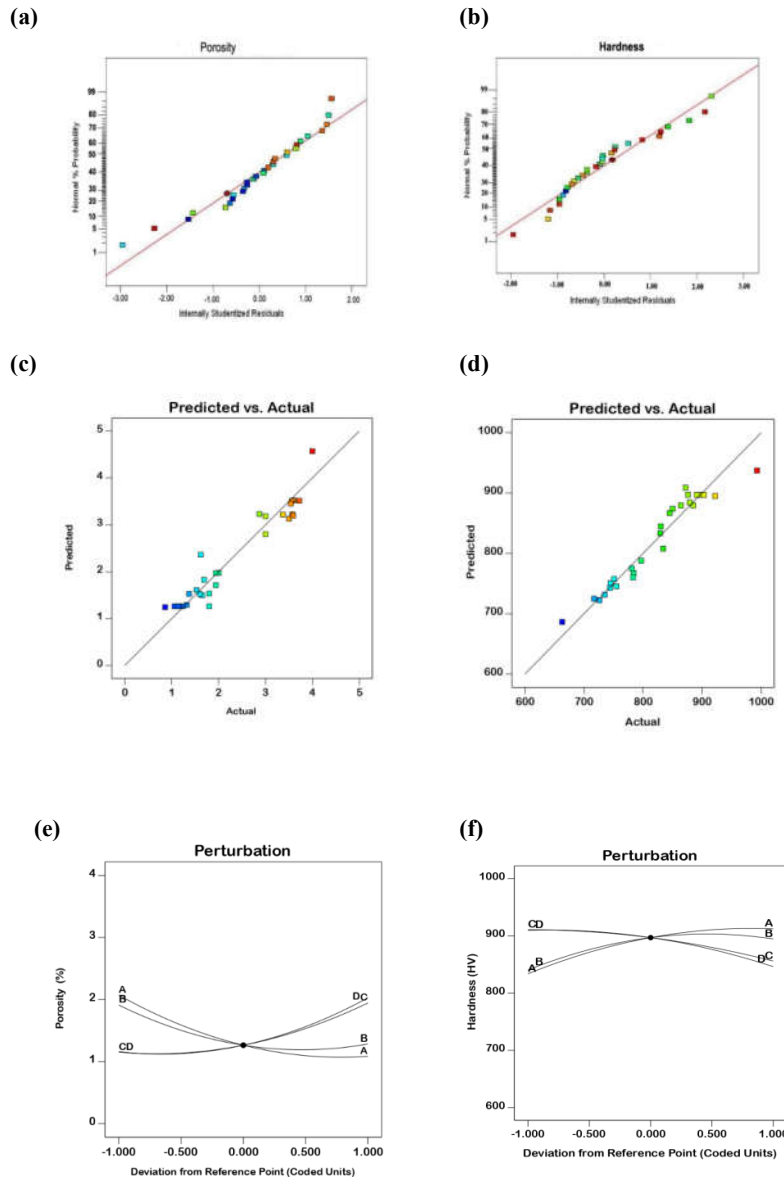


Figure 2. (a-b) Normal probability curve, (c-d) predicted vs actual graph, and (e-f) perturbation graph for porosity and hardness.

In each of the developed empirical observations, the lack of fit was not as important as expected. A high level of significance is shown by Fisher's Test statistic having a very low possibility value ($p_{model} > F = 0.0001$). The determination factor was employed to determine how well the model corresponded to the data (R^2). Just under one percent of the overall deviations

cannot be understood according to the observed relation based on the coefficient of determination R^2 value, which was higher than 0.99. The strong significance of Empirical correlations is shown by the magnitude-modified coefficient of determination, which is also extreme. The variations of the projected estimates from the perspective of design are compared with the mean prediction error to determine whether precision is enough. Additionally, a comparatively low coefficient of variance suggests that the trials were performed with greater accuracy and dependability. The improved correctness and repeatability of the performed trials are indeed indicated by the remarkably low coefficient of variation [26]. The answers shown in Figure 2(a–b) are indicated by the conventional probability plots. It is possible to determine from Figure 2(a–b) that residuals drop on an undeviating line, indicating that errors are supplied equally. According to Figure 2(c–d), which compares actual and expected values, there is a high correlation between approximated and expected values.

RESULTS AND DISCUSSION

The optical microstructure of the magnesium base, which exhibits equiaxed grains, is illustrated in Figure 3(a). The angular forms of the TiO_2 feedstock are illustrated in Figure 3(b). The X-ray diffraction analysis of the TiO_2 coating powder is illustrated in Figure 3(c). The TiO_2 coating was fabricated on the AZ81 Mg alloy, and the mean thickness of the coatings was maintained at $200 \pm 5 \mu\text{m}$.

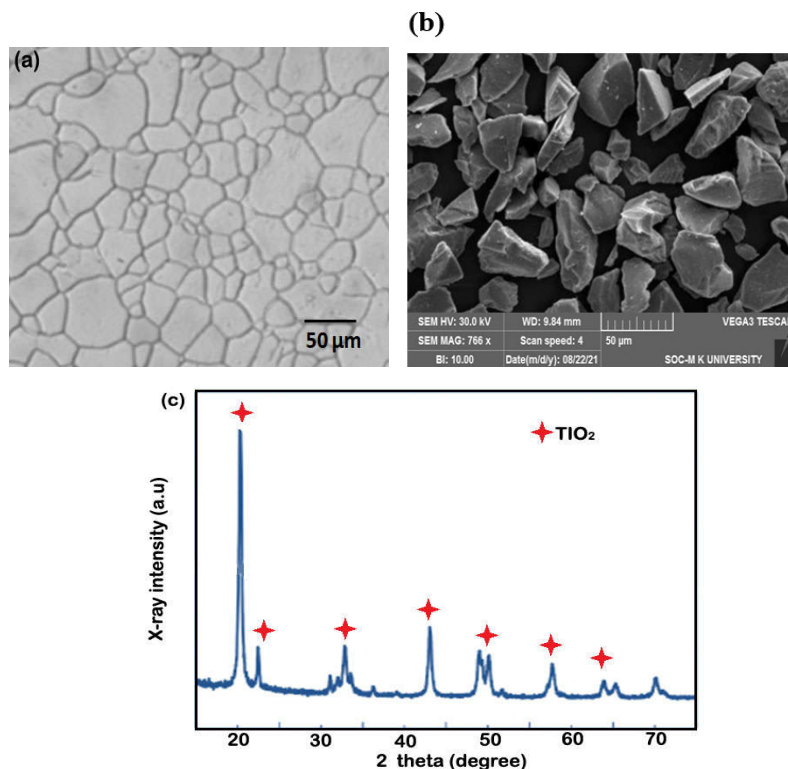


Figure 3. (a–b) optical microstructure of the magnesium base, and (c) X-ray diffraction analysis of the TiO_2 coating powder.

Observations made throughout the trial

LPG flow rate: whenever the flow rate falls below 62 lpm, several partially melted particulates are observed due to insufficient heat generation. If the LPG flow is greater than 70 lpm, more heat is already being produced, and the nozzles have been noticed to heat up. Oxygen flow rate: When the oxygen flow velocity is much less than 252 lpm, incomplete LPG burning has been observed, and if it reaches 268 lpm, more partially melted coating grains are found.

Powder feed rate: The lowest powder feed rate recorded was 28 gpm. If the speed of powder input reaches 48 lpm, the coating still includes partially melted particles. Spray distance: excess heat on the substrate has been noticed when the spray range is less than 216 mm, while poor coating was noticed when the range was longer than 240 mm.

To thoroughly melt the TiO₂ feed, the appropriate oxygen and LPG ratio is essential (the melting temperature of titania is 1855 °C). Poor coating, lowest thickness, and more partially melted grains have been noted when levels are increased or decreased.

The model that has been developed can be utilized to construct the plots for numerical simulations and to enhance results. These designs have been developed to keep the conversation going. In Figure 2(e-f), the perturbation graph indicates the impacts of the HVOF.

Processing variables for deposit porosity and micro-hardness were recently generated and displayed in Table 3. The perturbation plot is a significant graphical representation that offers observations of the response values in silhouettes. This chart shows the response modifications for each component deviating from the designated reference point despite holding the set point for all other factors. If a variable has a steep climb or curvature, the response is sensitive to the factors. The relatively flat stay is connected to the factor's lack of sensitivity to change.

Effect of hardness and porosity

The analysis of variance (ANOVA) applied to the values of F reveals that LPG flow velocity and spraying length have a significant influence on the porosity and hardness of the TiO₂ spray. As shown in the perturbation plot (Figure 2(e-f),) as process variables are expanded, porosity decreases, and when they are expanded higher, the porosity levels rise. A perturbation graph allowed us to determine that the decreased fuel flow rate created inefficient dissolving of the tiny particles, which resulted in high porosity and lower hardness. At a lower gas supply, the flame's temperature is low, which hinders the dissolution of TiO₂ (that melted at 1855 °C), the feeding, and particulate or droplet displacement at substrate impact, which results in incomplete filling, increased particle sizes, and a lower hardness value. It has been confirmed that the HVOF process performed at the required oxygen flow rate and pressure and that, under the prevailing circumstances, the heating rate would increase with such an increase in fuel gas flow.

In conclusion, a rise in the fuel gas flow increased the spray powder's melting condition. The temperature difference and velocity distribution improve with the rate of fuel usage. Higher particle velocity and temperature may improve inter-splat connection, coating porosity, and microhardness, though larger droplet viscosity will decrease as particle temperature rises. [29]. When it comes to coating qualities, physical and chemical conditions, including pressure, temperature, and flame velocity, are heavily affected by a variety of HVOF process factors, with oxygen flow velocity, fuel rate of flow, spray range, and powder particle size being the most critical.

Gas leaks may be controlled during the quick spread and quench of the splat, which might lead to a rise in the pressure of the gas in the splat core and the formation of a lean cap on a gas bubble. This excess hole would then boost porosity levels and lower hardness values [27]. It is apparent from the graph that oxygen flow rate affects combustion temperatures and velocity in a significant manner. The powders are warmed and rapidly accelerated by the combustion products during the HVOF spraying process. When there is enough oxygen to complete the combustion of

LPG, the flame temperature reaches its maximum. Oxygen flow velocity results in leftover oxygen that performs as a coolant gas and, as a response, encourages a decrease in combustion temperature [28]. By raising the flow rate of oxygen, the particle velocity and flame are also improved. This reduces the particle's residence time in the flame and, as a function, reduces the temperature of the molecule. Due to the excess LPG that acts as a cooling gas whenever the oxygen production rate is much lower, the flame temperature decreases [29]. Anyway, the lower or extreme oxygen content finds extra particles that are unmelted as a consequence of the coolant effect that takes place in the flame. Particle rebound may occur because all of these unmelted particles do not adhere to the material or previously accumulated surface. That decreases hardness and increases porosity.

The consequence of the feed rate of powder (curve of F) on the response is illustrated in Figure 2(e-f). The particles that should share the thermal and kinetic energy of flame are controlled by the variability in the powder feed rate, which also affects the particles' temperature and velocity. When the maximum feed rate is lower, the majority of the particles melt, creating a quench fracture that increases porosity and reduces hardness. Considering the other factors, the correct powder feed rate, the spray particles' molten degree, and the decrease in porosity, these will increase the hardness and reduce the porosity [28]. The differences in the consequences of spray distances (curve D) are displayed in Figure 2(e-f). It demonstrates how hardness rises as the distance of the spray grows to its highest level and then consequently drops. A smaller particle velocity towards the substrate was produced by a greater spraying range, which resulted in a coating with a lower frequency. Furthermore, by lowering the mean impact temperature change of the dewdrop with the system, a higher volume percentage of unmelted particles is produced. Both of these outcomes result in a significant rise in coating porosity.

According to reports, as the spray length increased, a supersonic jet continuously accelerated the particles, despite a retarding force from the entrainment atmosphere damaging the particles. As a result, the enthalpy of melted ceramic substances is nearly zero, and particles move more slowly. In these circumstances, the particles contacting the substrate won't be compressed to cover up the layers, leading to a much-reduced hardness and porosity value [29]. Reduced spray velocity initially increased the deposition rate, but issues developed with the substantially increased heat capacity. Coatings are hard, but quenching could cause fractures, which could also encourage porosity and decrease hardness. When spraying at the proper distance, the gas jet delivers the particles at a sufficient temperature and velocity. The reduction in porosity and high hardness were obtained because the ideal temperature allowed for more efficient packing of splats and better cohesiveness between splats [28].

Optimizing HVOF spray parameters

The surface response was computed because it was important for enhancement to identify how important aspects affect the researched response and to create an objective of enhancing the responses of interest to acquire optimal parameter values. Figures 4 (three-dimensional response surfaces) demonstrate the quadratic response equation for the porosity as solid surfaces in two-dimensional contour plots.

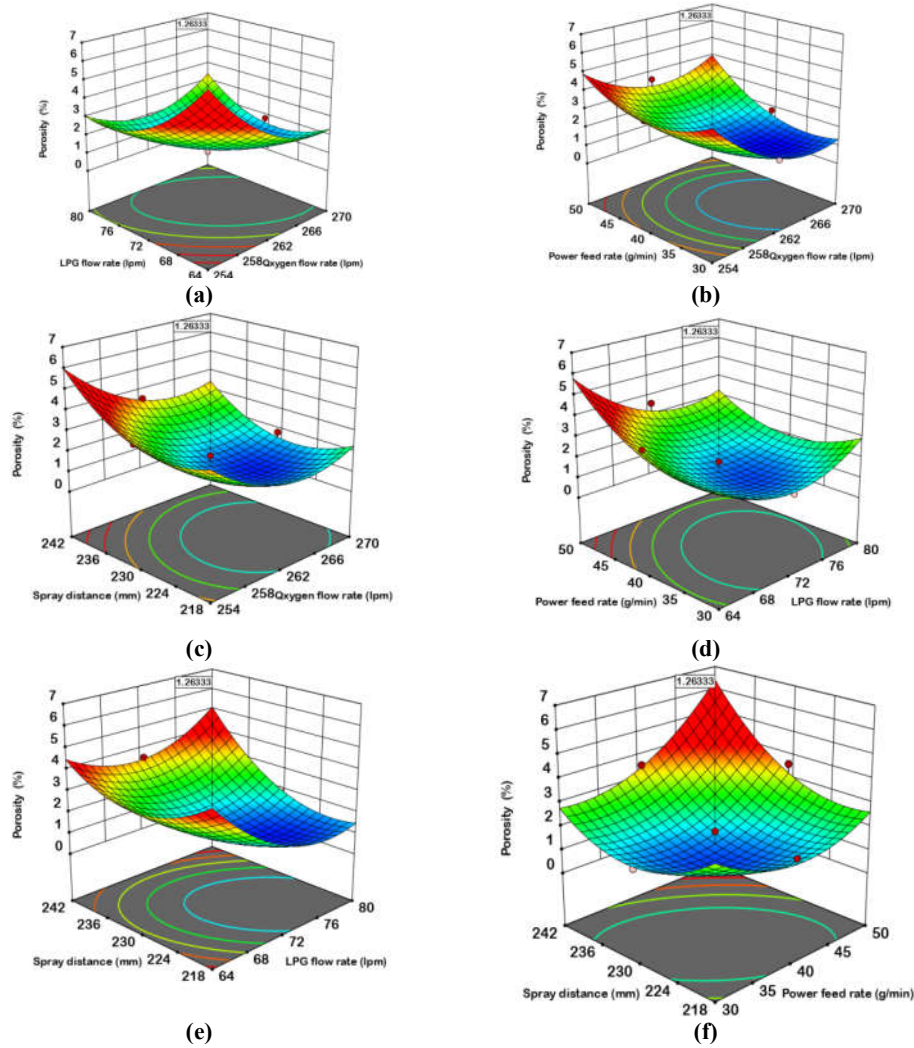


Figure 4. Response graphs for coating porosity.

Figure 5(a-f) depicts the multi-direction calibration curves of the polynomial response equation for the hardness, and Figure 5 depicts the three-dimensional response surfaces (a-f). For any portion of the experimental domain, these response contours can aid in response prediction (porosity and hardness) [26–29]. To graphically depict the area of the ideal factor settings, a contour map is created. Such a plot can be more complicated for second-order answers compared to first-order models' simple array of parallel lines. Characterizing the response surface close to a stationary point after one has been identified is typically necessary. During characterization, decide if the static position is a saddle point, the lowest reaction, or the peak reaction. Plotting contours is crucial for understanding the response surface [27–32].

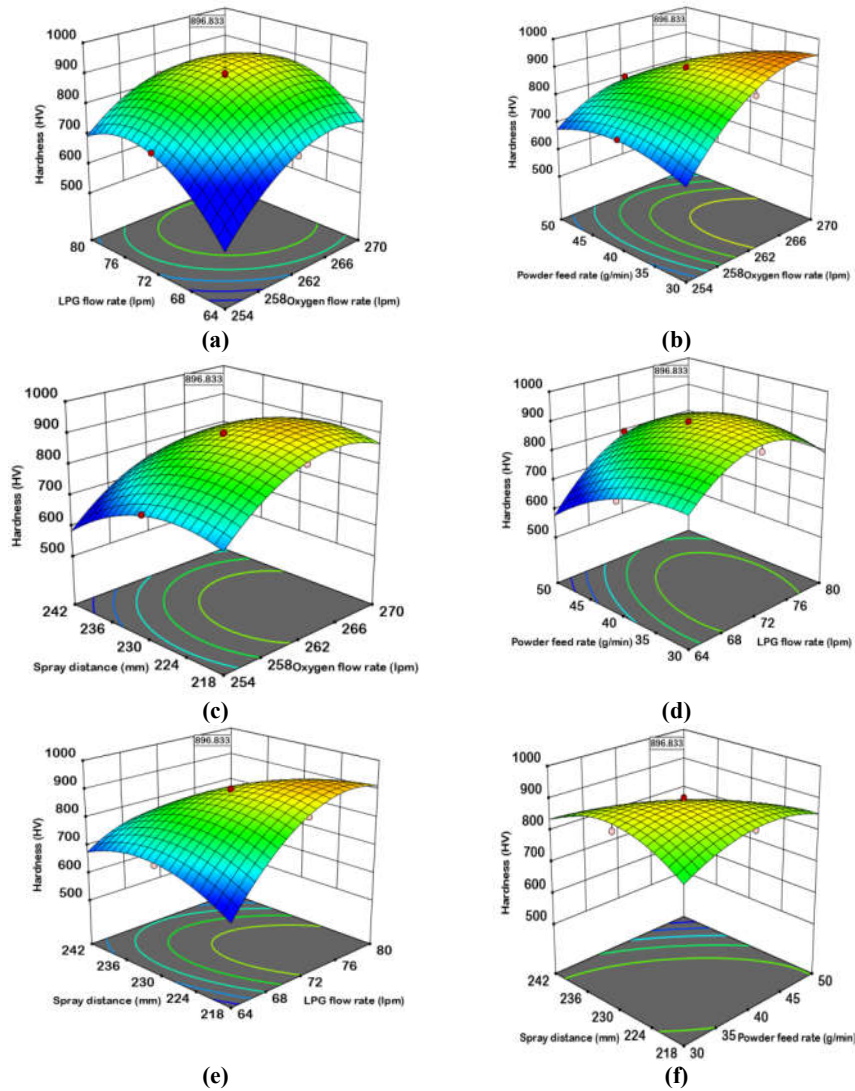


Figure 5. Response graphs for coating hardness.

As the values of the process parameters under consideration rise, the porosity drop hits a low point and then increases, as depicted in Figure 4. The lowest porosity is evident in the response plot's valley. According to the response graph, the LPG flow rate and spraying distance were the main determinants of porosity. When fuel flow and spray distance are ideal, the flame reaches greater temperatures and velocities, effectively depositing TiO_2 particles on the substrate. Interlayer porosity and the percentage of defrosted particles were thus decreased.

The SEM pictures of the TiO_2 coating's upper layer are shown in Figure 6(a). The coating was created at a greater fuel flow rate, as evidenced by certain agglomerates of normal size that solidified before contact with the previously applied coating. The surface of the sprayed coating

shows that the particles are closely integrated when it is in its ideal form, and the coating appears to be quite dense. The micro-hardness of the coatings was significantly influenced by porosity because higher density is produced by lower porosity. The pinnacle of the reaction demonstrates the high hardness, as shown by the plot and three-dimensional response levels for the response hardness from the regression analysis. As the values of the elements under examination rise, the strength of the TiO₂ coating reaches its peak and then declines. The overlay plots represent the outcomes of the graphical optimization. These plots are quite useful for selecting the HVOF spray parameter values that would provide a certain response value for this kind of material in the TiO₂ coating manufacturing sector. The regions that fulfil the suggested criteria and optimised values are shown in the overlay plot (Figure 6(c)) as yellow-shaded areas. The fuel flow rate and spray distance affect the coating's microhardness value. The microhardness of the TiO₂ coating was measured in this investigation to be between 663 and 923 HV0.3. A dense and tougher coating was produced when conditions were ideal.

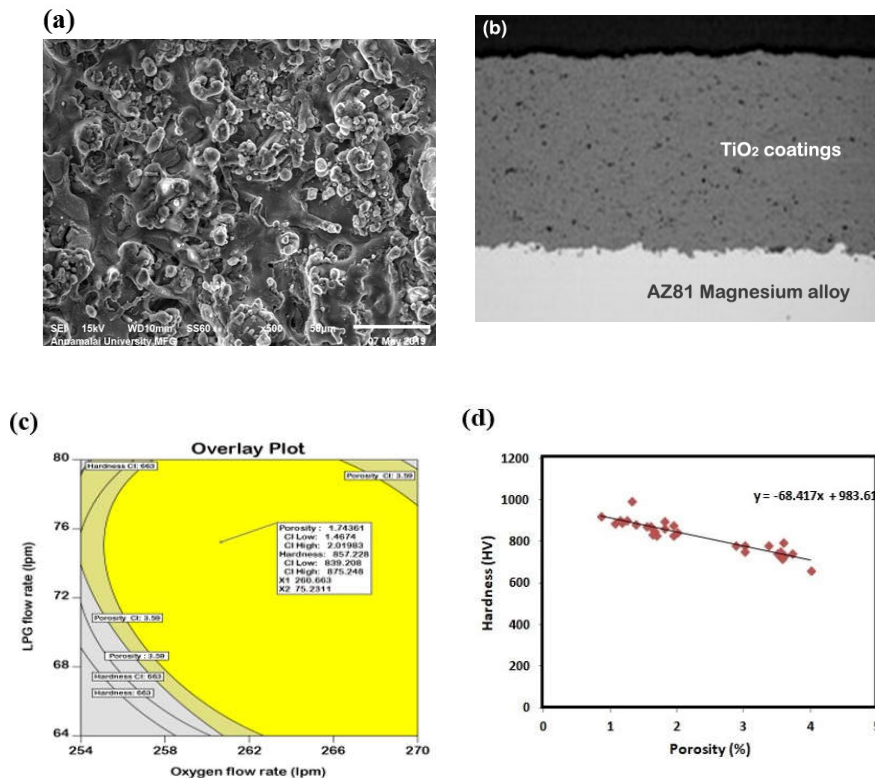


Figure 6. SEM morphology of TiO₂ coating (a) top surfaces, (b) cross-section, (c) overlay plot, and (d) relationship between hardness and porosity.

This could be explained by a higher flame jet temperature raising the impacting particle temperature, which then lowers the porosity level due to the interaction of cohesiveness and produces a greater hardness. In the description above, arithmetical optimization was carried out

by solving equations and examining the responsive surfaces' profiles, and creating related contour plots.

The response values were calculated using the following configurations: oxygen composition of 266 lpm, LPG composition of 68 lpm, powder feed rate of 35 gpm, and spray distance of 236 mm. The hardness value for this metric is 922 HV0.3, while the lowest porosity value is 0.86 volume percent. Figure 6(b), which depicts the cross-sectional morphology of the titanium oxide coating at optimal conditions, shows that the coating is extremely dense and homogenous.

Relationship between porosity and hardness

By integrating the experiment results in a straight line, it is possible to determine the relationship between hardness and porosity (Figure 6(d)). The regression relation defines the perfect line.

$$\text{Microhardness (HV)} = 98.61 - 68.471 (\text{Porosity}) \quad (6)$$

The finding of the coefficient equation's curve (-68.471) is low, showing the hardness value increases as permeability decreases. This estimated regression coefficient may describe 89% of both cumulative total squares, as indicated by a coefficient of estimation (R^2) = 89%. An estimated regression equation's efficiency of fitting is judged by its coefficient of estimation, R^2 . To calculate the average value of hardness values for the known range of coated permeability and also to predict the inherent worth of the spraying hardness for a specific significance of spraying porosity levels, use the regression function polynomial line equations.

The reliability of the correlation test is indicated by confidence intervals (CI) and predictive intervals (PI). The average values of y for the given values of x serve as the interval analysis for the confidence level. Prediction intervals are the sector that estimates a single value of y for a particular value of x.

Instead of a particular value of covering permeability, the calculated regression coefficient provides a ballpark approximation of the average microhardness values. Since the average values of microhardness could be calculated with greater accuracy than the individual values, CI and PI are distinguished from one another. By predicting the outcome of the random vector rather than evaluating its average value, the bigger PI illustrates the enhanced uncertainty that results. Figure 6(d) shows that the interval becomes narrower as the value approaches X (2.68%).

Research conducted through experimentation shows that the porosity is typically between 1 and 4%. Generally, porosity and hardness properties are strongly correlated. The porosity significantly affects the hardness. When the porosity and microcracks diminish, the hardness of the coating rises significantly. Furthermore, porosity has a significant impact on hardness.

CONCLUSIONS

(1) Empirical models were utilized to predict the porosity and microhardness of TiO₂ coatings, considering various spraying variables such as fuel and oxygen flow rates, powder feed rate, and spraying distance. (2) Among the four examined HVOF process variables, the coating qualities were found to be most influenced by fuel flow, followed by spraying distance, oxygen flow rate, and powder feed rate. (3) Linear regression equations were developed to describe the porosity and microhardness of the TiO₂ coating applied via HVOF. These relationships, established at a 95% confidence level, offer accurate predictions for substrate porosity and microhardness of TiO₂.

The coating achieved with optimal spray parameters demonstrates a lower surface porosity of 0.86 vol.% and attains a higher hardness of 922 HV compared to other coated samples. Validation through the response graph confirms these findings. As a result, the optimized parameters for depositing TiO₂ consist of an oxygen flow rate of 266 lpm, an LPG flow rate of 68 lpm, a powder feed rate of 35 g/min, and a spray distance of 236 mm.

REFERENCES

- Diebold, U. The surface science of titanium dioxide. *Surf. Sci. Rep.* **2003**, 48, 53-229.
- Kemmitt, T.; Al-Salim, N.I.; Waterland, M.; Kennedy, V.J.; Markwitz, A. Photocatalytic titania coatings. *Curr. Appl. Phys.* **2004**, 4, 189-192.
- Hu, J.J.; Liao, J.; Yang, X.; Zeng, J.; Li, H.; Song, B.; Jin, Y. Microstructure and properties of Al-coating on AZ31 magnesium alloy prepared by pack-cementation. *Trans. Nonferrous Met. Soc. China* **2022**, 32, 493-502.
- Goyal, K. Mechanical properties and erosive behaviour of 10TiO₂-Cr₂O₃ coated CA6NM turbine steel under accelerated conditions. *World J. Eng.* **2019**, 16, 64-70.
- Lu, Y.-P.; Li, M.-S.; Li, S.-T.; Wang, Z.-G.; Zhu, R.-F. Plasma-sprayed hydroxyapatite + titania composite bond coat for hydroxyapatite coating on magnesium substrate. *Biomaterials* **2004**, 25, 4393-4403.
- Tomaszek, R.; Pawlowski, L.; Gengembre, L.; Laureyns, J.; Le Maguer, A. Microstructure of suspension plasma sprayed multilayer coatings of hydroxyapatite and magnesium oxide. *Surf. Coat. Technol.* **2007**, 201, 7432-7440.
- Prasad, R.V.; Rajesh, R.; Thirumalaikumarasamy, D.; Ashokkumar, M.; Rajakumar, S. Multi response optimization of hvof process parameters in low carbon steels. *Sādhanā* **2022**, 47, 265.
- Goller, G. The effect of bond coat on mechanical properties of plasma sprayed bioglass-magnesium coatings. *Ceram. Int.* **2004**, 30, 351-355.
- Oktar, F.N.; Yetmez, M.; Agathopoulos, S.; Goerne, T.M.L.; Goller, G.; Ipeker, I.; Ferreira, J.M.F. Bond-coating in plasma-sprayed calcium-phosphate coatings. *J. Mater. Sci. Mater. Med.* **2006**, 17, 1161-1171.
- Kurzweg, H.; Heimann, R.B.; Troczynski, T.; Wayman, M.L. Development of plasma-sprayed bioceramic coatings with bond coats based on titania and zirconia. *Biomaterials* **1998**, 19, 1507-1511.
- Jeffery, B.; Pepler, M.; Lima, R.S.; McDonald, A. Bactericidal effects of HVOF-sprayed nanostructured TiO₂ on pseudomonas aeruginosa. *J. Therm. Spray Technol.* **2009**, 19, 344-349.
- Clavijo-Mejía, G.A.; Espinosa-Arbeláez, D.G.; Hermann-Muñoz, J.A.; Giraldo-Betancur, A.L.; Muñoz-Saldaña, J. Effect of HVOF process parameters on TiO₂ coatings: An approach using DoE and first-order process maps. *J. Therm. Spray Technol.* **2019**, 28, 1160-1172.
- Lima, R.S.; Marple, B.R. From APS to HVOF spraying of conventional and nanostructured titania feedstock powders: A study on the enhancement of the mechanical properties. *Surf. Coat. Technol.* **2006**, 200, 3428-3437.
- Bansal, P.; Shipway, P.H.; Leen, S.B. Effect of particle impact on residual stress development in HVOF sprayed coatings. *Proc. Int. Therm. Spray Conf.* **2006**, 15, 570-575.
- Vignesh, P.; Ramanathan, S.; Ashokkumar, M.; Sonar, T.; Ananthi, V. Microstructure, mechanical, and electrochemical corrosion performance of Ti/HA (hydroxyapatite) particles reinforced Mg-3Zn squeeze casted composites. *Int. J. Metalcast.* **2024**, 18, 1348-1360.
- Murugan, K.; Ragupathy, A.; Balasubramanian, V.; Sridhar, K. Optimizing HVOF spray process parameters to attain minimum porosity and maximum hardness in WC-10Co-4Cr coatings. *Surf. Coat. Technol.* **2014**, 247, 90-102.
- Noreen, S.; Wang, E.; Feng, H.; Li, Z. Functionalization of TiO₂ for better performance as orthopedic implants. *Materials* **2022**, 15, 6868.
- Hernández-Montes, V.; Betancur-Henao, C.P.; Santa-Marín, J.F. Titanium dioxide coatings on magnesium alloys for biomaterials: A review. *Dyna* **2017**, 84, 261-270.
- Fauchais, P.; Fukumoto, M.; Vardelle, A.; Vardelle, M. Knowledge concerning splat formation: An invited review. *J. Therm. Spray Technol.* **2004**, 13, 337-360.
- Ribu, D.C.; Rajesh, R.; Thirumalaikumarasamy, D.; Kaladgi, A.R.; Saleel, C.A.; Nisar, K.S.; Afzal, A. Experimental investigation of erosion corrosion performance and slurry erosion mechanism of HVOF sprayed WC-10Co coatings using design of experiment approach. *J. Mater.*

- Res. Technol.* **2022**, 18, 293-314.
21. Palanisamy, K.; Gangolu, S.; Antony, J.M. Effects of HVOF spray parameters on porosity and hardness of 316L SS coated Mg AZ80 Alloy. *Surf. Coat. Technol.* **2022**, 448, 128898.
 22. Friis, M.; Persson, C. Control of thermal spray processes by means of process maps and process windows. *J. Therm. Spray Technol.* **2003**, 12, 44-52.
 23. Valarezo, W.; Choi, W.B.; Chi, W.; Gouldstone, A.; Sampath, S. Process control and characterization of NiCr coatings by HVOF-DJ2700 system: A process map approach. *J. Therm. Spray Technol.* **2010**, 19, 852-865.
 24. Pierlot, L.; Pawlowski, L.; Bigan, M.; Chagnon, P. Design of experiments in thermal spraying: A review. *Surf. Coat. Technol.* **2008**, 202, 4483-4490.
 25. Hasan, S.; Stokes, J. Design of experiment analysis of the Sulzer Metco DJ high velocity oxy-fuel coating of hydroxyapatite for orthopedic applications. *J. Therm. Spray Technol.* **2010**, 20, 186-194.
 26. Forghani, S.M.; Ghazali, M.J.; Mughtar, A.; Daud, A.R.; Yusoff, N.H.N.; Azhari, C.H. Effects of plasma spray parameters on TiO₂-coated mild steel using design of experiment (DoE) approach. *Ceram. Int.* **2013**, 39, 3121-3127.
 27. Mohankumar, A.; Thirumalaikumarasamy, D.; Sampath kumar, D.; Ranganathan, S.; Sonar, T.; Ivanov, M.; Vignesh, P.; Pavendhan, R.; Xu, J. Optimization of cold spray process inputs to minimize porosity and maximize hardness of metal matrix composite coatings on AZ31B magnesium alloy. *J. Nanomater.* **2022**, 7900150.
 28. Mohankumar, A.; Thirumalaikumarasamy, D.; Sonar, T.; Ivanov, M.; Vignesh, P.; Pavendhan, R.; Xu, J. Cold spray processing of AA2024/Al₂O₃ coating on magnesium AZ31B alloy: Process parameters optimization, microstructure and adhesive strength performance of coating. *Int. J. Lightweight Mater. Manuf.* **2023**, 6, 516-526.
 29. Seshaiyah, S.; Sampathkumar, D.; Mariappan, M.; Mohankumar, A.; Balachandran, G.; Kaliyamoorthy, M.; Gopal, R. Optimization on material removal rate and surface roughness of stainless steel 304 wire cut EDM by response surface methodology. *Adv. Mater. Sci. Eng.* **2022**, 6022550.
 30. Mathivanan, K.; Thirumalaikumarasamy, D.; Ashokkumar, M.; Deepak, S.; Mathanbabu, M. Optimization and prediction of AZ91D Stellite-6 coated magnesium alloy using box behnken design and hybrid deep belief network. *J. Mater. Res. Technol.* **2021**, 15, 2953-2969.
 31. Sivashankar, N.; Thanigaivelan, R.; Saravanan, K.G. Electrochemical micromachining and parameter optimization on AZ31 alloy—ANN and TOPSIS techniques. *Bull. Chem. Soc. Ethiop.* **2023**, 37, 1263-1273.
 32. Tharaknath, S.; Rahamathullah, I. Mechanical, chemical, metallurgical characteristics under HBSS solution and optimization of AZ91D-Ti functional graded composites using TOPSIS. *Bull. Chem. Soc. Ethiop.* **2023**, 37, 77-89.